J Nanostruct 17(1): 225-237, Winter 2027

RESEARCH PAPER

Enhancing the Efficiency and Stability of Perovskite Solar Cells Using Nano polymer Fiber Scaffolds

Mahr A. Athal [1], Tebark Abd Zaid Hassoun [2], Niran Salim Ali [3], Mohamed A. Shaheed [4]*

[1] *Department of physics, College of Eudcation in Qurna, University of Basrah, Basra, Iraq*
[2] *Department of Medical Physics, College of Science, University of Hilla, Iraq*
[3] *Department of Physics, College of Science, University of Kerbala, Iraq*
[4] *Department of Physic, College of Education, University of Al-Qadisiyah, Iraq*

ARTICLE INFO

Article History:
Received 27 July 2026
Accepted 03 November 2026
Published 01 January 2027

Keywords:
3D Nanocomposite
High Efficiency
Intrinsic Encapsulation
Nanofiber Scaffold
Perovskite Solar Cells

ABSTRACT

Perovskite solar cells (PSCs) currently experience a significant trade-off between performance and durability. Moisture is known for damaging PSCs over time. However, when the active layer is changed from traditional 2D to holistic 3D and integrated a polystyrene nanofiber scaffold, system can create a multifunctional 3D nanocomposite that, at the same time, directs crystal growth, while providing intrinsic environmental protection. The use of this nanofiber scaffold permits the growth of very large-grain (order of a micron), high-crystal quality and inhibits the formation of PbI_2 impurities. As a result, scaffold-enhanced PSCs reach remarkable power conversion efficiency (PCE) of 22.81% (average of 22.38%) and significantly exceed the performance of reference cells (average of 19.45%) due to increased open-circuit voltage (1.15 V) and fill factor (82.5%). Importantly, the 3D scaffold also provides an intrinsic encapsulation mechanism. Unencapsulated PSCs retain over 90% of their initial efficiency after 500 h at 50-60% relative humidity, while reference cells degrade to <20%. These results demonstrate the power of 3D structural engineering using nanofiber scaffolds as an effective method for the fabrication of highly efficient and durable PSCs and set the stage for commercially viable perovskite-based photovoltaics.

How to cite this article
Athal M., Zaid Hassoun T., Salim Ali N., Shaheed M. Enhancing the Efficiency and Stability of Perovskite Solar Cells Using Nano polymer Fiber Scaffolds. J Nanostruct, 2027; 17(1):225-237. DOI: 10.22052/JNS.2027.01.021

INTRODUCTION

The today's world stands at a critical crossroads, where the relentless increase in global energy demand, driven by population growth and industrial expansion, exerts immense pressure on traditional energy resources. The near-absolute reliance on fossil fuels has not only raised geopolitical and security concerns related to supply sustainability but has also led to an unprecedented environmental crisis. The Intergovernmental Panel on Climate Change (IPCC) confirms that greenhouse gas emissions from burning fossil fuels are the primary driver of global warming, threatening the stability of global ecosystems [1]. In this context, the transition to renewable energy sources is no longer a luxury but a strategic imperative. Solar energy emerges as the most abundant and democratic of these sources, offering the potential for clean electricity generation almost anywhere. Although crystalline

* *Corresponding Author Email: mahr.athal@uobasrah.edu.iq*

This work is licensed under the Creative Commons Attribution 4.0 International License.
To view a copy of this license, visit http://creativecommons.org/licenses/by/4.0/.

silicon cells have established the foundations of the photovoltaic industry and proven their reliability, their complex manufacturing processes, which require high temperatures and enormous energy input, along with their mechanical rigidity, place constraints on the potential for radical cost reduction and limit their applications in flexible and portable electronics [2]. This technological gap is precisely what has paved the way for the emergence of third-generation solar cells, chief among them perovskite solar cells (PSCs), which hold the promise of revolutionizing the energy sector. Since their initial emergence in 2009 [3], PSCs have radically transformed the landscape of photovoltaic research. In a record time of just over a decade, the power conversion efficiency of these cells has skyrocketed from 3.8% to certified values exceeding 26.1% [4]. The secret to this superior performance lies in a set of exceptional physical properties inherent to hybrid perovskite materials (with the general formula ABX_3). They possess an immense optical absorption coefficient (~10^5 cm^{-1}) across the visible spectrum, allowing for the fabrication of very thin active films (less than 500 nm) capable of efficiently absorbing most sunlight, which reduces material consumption and cost [5]. Furthermore, these materials exhibit excellent charge transport properties, characterized by long electron and hole diffusion lengths (exceeding a micrometer) and low exciton binding energy, ensuring that free charge carriers are generated and collected with high efficiency. However, behind this impressive success story lies a major obstacle hindering the technology's transition from the laboratory to the market: operational instability. This is a multifaceted problem arising from a complex interplay of extrinsic and intrinsic factors. Externally, the perovskite structure, particularly its ionic organic components, shows extreme sensitivity to atmospheric moisture, where its reaction with water leads to the material's irreversible decomposition into lead iodide (PbI_2), thereby destroying its photovoltaic structure [6]. Oxygen, especially in the presence of light, also contributes to accelerating this degradation. Internally, the material suffers from thermal instability at relatively high operating temperatures (above 85°C) and from the phenomenon of ion migration (especially halide ions) under the influence of an electric field, which causes hysteresis in electrical measurements and creates recombination pathways for charges [7]. Additionally, the quality of the perovskite film itself plays a crucial role; films prepared *via* conventional solution-based methods often contain structural defects such as pinholes and non-passivated grain boundaries, which act as active recombination centers and weak points for moisture and oxygen to infiltrate the film.

To confront these dual challenges, the need for high-quality films (for efficiency) and the need for effective protection (for stability), nanomaterial engineering has emerged as a powerful tool. Among the innovative approaches, the integration of nanopolymer fiber scaffolds, typically prepared *via* electrospinning, presents a promising and unique solution. Firstly, from the perspective of efficiency and morphology enhancement: The porous nanofiber network acts as a 3D template or scaffold during the perovskite crystallization process, instead of random crystallization on a flat substrate. The growth of perovskite crystals is guided within the pores of this nanoscale network. This process can lead to the formation of larger and more oriented crystalline grains and reduce the density of grain boundaries, which are major sources of charge loss. Furthermore, this scaffold aids in forming a continuous and pinhole-free film, which improves the charge extraction process and reduces leakage currents, thereby increasing the overall efficiency and fill factor of the solar cell [8]. Secondly, from the perspective of stability and protection: The polymer nanofibers offer a unique intrinsic encapsulation mechanism, by selecting a suitable polymer with a hydrophobic nature, such as polymethyl methacrylate (PMMA) or polystyrene (PS). The nanofiber network encapsulates and surrounds the growing perovskite crystals. This nanoscale sheath acts as an effective barrier, preventing water molecules from reaching the sensitive perovskite material, which significantly enhances the cell's stability against moisture [9]. Additionally, this polymer network can "immobilize" the mobile ions within the crystal structure, thus mitigating the destructive phenomenon of ion migration and improving the operational stability of the cell under continuous illumination and heat. The presence of these fibers also imparts superior mechanical flexibility and durability to the hybrid film, which is crucial for flexible solar cell applications [10].

Based on the foregoing, this research aims to conduct a systematic and comprehensive investigation into the effect of integrating

CC BY

nanopolymer fiber scaffolds into the active layer of perovskite solar cells, to achieve the dual objective of enhancing both efficiency and stability simultaneously. The specific objectives are: (1) Fabricating polymer nanofiber scaffolds with controlled diameters and porosity using the electrospinning technique, (2) Integrating these scaffolds into the perovskite solar cell fabrication process to study their effect as a crystallization template, (3) Characterizing the morphological, crystalline, and optical properties of the resulting hybrid layer, (4) Evaluating the photovoltaic performance of the enhanced cells and comparing it to reference cells and (5) Conducting an in-depth study of the long-term stability of the cells under various stress conditions (humidity, heat, illumination).

The intrinsic significance of this work lies in the fact that it does not merely offer an incremental improvement, but rather proposes a paradigm shift in the design of the active layer itself, from a two-dimensional thin film to a three-dimensional nano-hybrid structure. The success of this strategy could provide a practical and scalable pathway for producing PSCs that combine high efficiency, low cost, and long-term reliability, thereby accelerating their potential adoption as a key technology in the global sustainable energy landscape.

The immense and continuous progress in PSCs technology has pivoted on understanding and mastering the physicochemical phenomena, occurring at the internal interfaces. These nanoscale regions, which separate the light-absorbing perovskite layer from the selective charge transport layers, are the critical arenas that determine the fate of photogenerated charge carriers. Efficient charge extraction occurs here, but conversely, the majority of non-radiative recombination losses also originate from structural and chemical defects concentrated at these very interfaces. This scientific reality has led to the dominance of "interface engineering" strategies in the research landscape, which have reached unprecedented levels of precision and efficacy, particularly with the advent of the self-assembled monolayer (SAM) revolution.

SAMs have proven their superior ability to transform an imperfect, defect-rich interface into a nearly electronically ideal surface. These brilliantly designed organic molecules act as a precise chemical bridge, passivating surface defects like undercoordinated lead ions, modulating the surface work function to create optimal energy level alignment, and minimizing barriers to charge extraction. The success of this approach has been demonstrated in a wide array of pioneering studies, where SAMs have been used to suppress the destructive oxidation at the NiO_x interface in highly sensitive tin-based perovskite cells [10], and where "co-adsorption" strategies combining different molecules have been developed to achieve multifunctionality in a single layer [11]. Tailored hole-selective molecules and others designed for precise regulation of the interface's electronic properties have led to effective defect passivation and quantum leaps in performance [12-14]. This research trajectory has culminated in record-breaking efficiencies and stabilities

Table 1. A comparative summary of advanced interface engineering strategies using SAMs in PSCs.

Core Outcome Achieved	Target Cell Type	Key Physicochemical Mechanism	Molecular Strategy / Key Material	Reference
Reduction in V_oc loss and enhanced chemical stability	Tin-based and Inverted PSCs	Defect passivation, oxidation suppression, energy level alignment	Various SAMs on HTL interface (e.g., NiO_x)	[10-14]
Achievement of world-record operational efficiency and stability	Inverted (p-i-n) PSCs	Formation of defect-free buried interface, strengthened bonding	Molecular hybrids and enhanced self-assembly	[15, 19]
Ideal current matching and increased dual-junction cell efficiency	Perovskite/Silicon Tandem	Ensuring high transparency and ideal ohmic contact, reducing recombination losses	SAMs in tandem cell interconnect layer	[16, 23]
Significant improvement in the stability and performance of tin-based cells	Mixed Tin-Lead (Sn-Pb) PSCs	Interface regulation, inhibition of Sn^{2+} oxidation, crystallization guidance	SAMs tailored for tin-lead cells	[17, 18]
Vast increase in mechanical durability and bending tolerance	Flexible Perovskite Solar Cells	Enhancing interlayer adhesion, distributing mechanical stress	SAMs in flexible devices	[20]
Improved film quality and enhanced phase and environmental stability	Inorganic ($CsPbI_3$), wide-bandgap	Control of phase homogeneity, passivation of surface defects	SAMs for inorganic & wide-bandgap cells	[21, 22]

CC BY

reported in top-tier scientific journals such as *Nature* and *Science*, cementing the status of SAMs as an indispensable tool [15, 16], as summarized in Table 1. The versatility of this technique has allowed for its broad application, encompassing complex tandem cells [17, 18], unstable mixed tin-lead perovskites [19-21], and even flexible devices [22].

However, despite this resounding success, the interface engineering paradigm as a two-dimensional surface treatment is a problem that extends its dimensions to the entire volume of the active layer. It addresses the symptoms that manifest at the surface, but it does not treat the root causes embedded within the bulk structure of the film. This is precisely where the profound knowledge gap lies, which this research directly aims to address. A monomolecular layer cannot dictate the crystallization process deep within the film, leaving the bulk structure prone to the formation of random grain boundaries that act as fast conduits for charge recombination and moisture ingress. Furthermore, it offers no protection for the top surface of the perovskite, nor does it contribute to enhancing the mechanical toughness of the inherently brittle film. From this vantage point, our research title, "enhancing the efficiency and stability of PSCs using nanopolymer fiber scaffolds," does not merely propose an incremental improvement but rather a paradigm shift in design philosophy: a transition from 2D surface engineering to 3D structural engineering. The integration of a nanopolymer fiber scaffold within the perovskite layer transforms the thin film from a simple deposited layer into a 3D nanocomposite material with multiple, integrated functionalities. This scaffold does not operate at a single interface but permeates the entire volume of the active layer to perform three vital functions. First, it acts as a structural scaffold, providing a 3D template for the crystallization process, guiding the growth of larger, more uniform grains

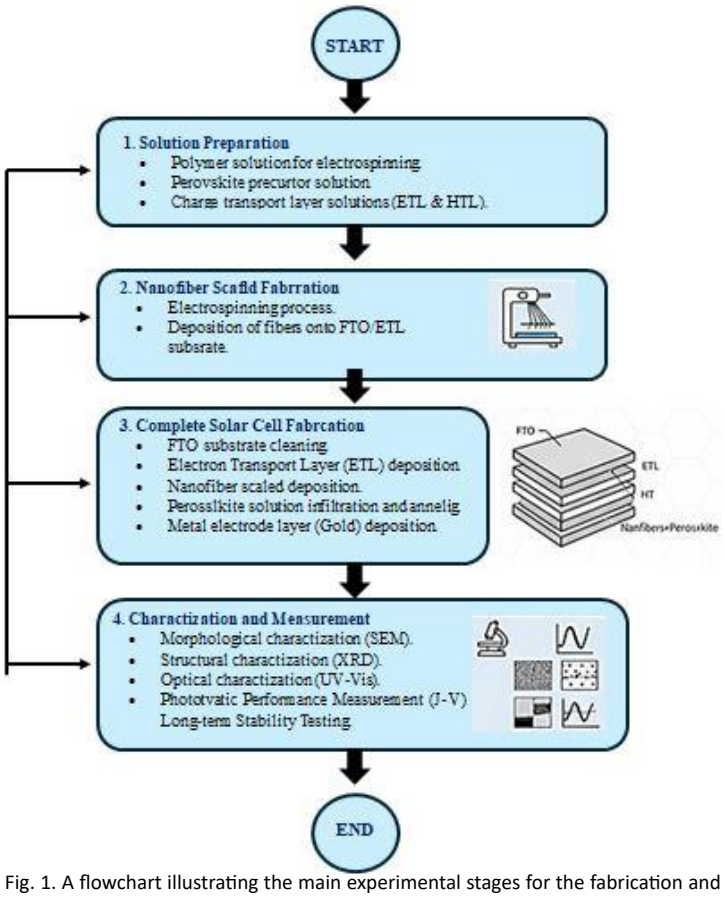


Fig. 1. A flowchart illustrating the main experimental stages for the fabrication and characterization of nanofiber-enhanced PSCs.

CC BY

and reducing the density of grain boundaries throughout the entire film volume. Second, the hydrophobic polymer fiber network serves as an intrinsic encapsulation system, enveloping the nascent crystals and providing immediate and comprehensive protection against moisture attack from all directions, not just from the bottom. Third, this network functions as a mechanical reinforcement framework, imparting exceptional flexibility and durability to the composite film, enabling it to withstand mechanical stresses during fabrication and operation.

Therefore, this research does not contradict the importance of interface engineering but rather complements and elevates it to the next level. It aims to construct a strong, integrated "building," not merely to perfect its foundation. By engineering the very structure of the active layer at the nanoscale, we aspire to address the challenges of efficiency and stability at their structural root, offering a holistic solution that paves the way for truly reliable and high-performance PSCs.

MATERIALS AND METHODS

Methodological and Experimental Roadmap

This section provides a meticulous and detailed account of all experimental procedures and materials employed in the context of this research. It begins with the selection and characterization of primary chemical reagents, progresses through the precise fabrication processes for both the nanopolymer fiber scaffolds and the complete PSCs, and concludes with the advanced characterization techniques utilized to evaluate the structural, optical, and electrical properties of the prepared samples. The methodology was designed to ensure the highest levels of accuracy and reproducibility and to facilitate a fair and direct scientific comparison between solar cells enhanced with nanofiber scaffolds and their conventional, reference counterparts. Fig. 1 presents a sequential flowchart that outlines the main stages of the experimental work, serving as the roadmap followed to achieve the research objectives, from the preparation of initial solutions to the final performance and stability measurements of the fabricated devices.

Chemicals and Materials

For all experimental stages, high-purity chemical reagents were used to ensure the accuracy of the results and to minimize the influence of impurities. All materials were used as received from the suppliers without any further purification. Table 2 provides a detailed list of the primary chemicals used in this research, specifying their chemical formulas, purity grades, and suppliers. Polystyrene was chosen for the fabrication of the nanofiber scaffolds due to its excellent hydrophobic nature, its solubility in common organic solvents, and its insulating properties, which make it well-suited for the electrospinning process. For the active layer, a mixed-cation (FA/MA/Cs) hybrid perovskite composition was selected to achieve an optimal

Table 2. List of primary chemicals used in the research.

Material	Chemical Formula	Purity (%)	Supplier
Nanoscaffold Materials			
Polystyrene (PS)	$(C_8H_8)_n$	M.W. ~350,000	Sigma-Aldrich
Dimethylformamide (DMF)	C_3H_7NO	≥ 99.8	Sigma-Aldrich
Toluene	C_7H_8	≥ 99.7	TCI
Perovskite Precursors			
Formamidinium Iodide (FAI)	CH_5IN_2	≥ 99.99	Greatcell Solar
Methylammonium Bromide (MABr)	CH_6BrN	≥ 99.99	Greatcell Solar
Lead (II) Iodide (PbI_2)	PbI_2	≥ 99.99	TCI
Lead (II) Bromide ($PbBr_2$)	$PbBr_2$	≥ 99.99	TCI
Cesium Iodide (CsI)	CsI	≥ 99.99	Sigma-Aldrich
Dimethyl Sulfoxide (DMSO)	C_2H_6OS	≥ 99.9	Sigma-Aldrich
Charge Transport Materials			
Tin (IV) Oxide Nanoparticle Ink (SnO_2)	SnO_2 (15% in H_2O)	-	Alfa Aesar
Spiro-OMeTAD	$C_{81}H_{68}N_4O_8$	≥ 99.5	Lumtec
Lithium bis(trifluoromethanesulfonyl)imide (Li-TFSI)	$CF_3SO_2NLiSO_2CF_3$	≥ 99.0	Sigma-Aldrich
4-tert-Butylpyridine (t-BP)	$C_9H_{13}N$	96	Sigma-Aldrich
Solvents and Other Materials			
Chlorobenzene	C_6H_5Cl	≥ 99.8	Sigma-Aldrich
Isopropanol	C_3H_8O	≥ 99.7	Sigma-Aldrich
Acetone	C_3H_6O	≥ 99.5	Sigma-Aldrich

CC BY

balance between high efficiency and phase stability.

Preparation of Polymeric Nanofiber Scaffolds via Electrospinning

Polystyrene nanofiber scaffolds were prepared using the electrospinning technique, as an effective and low-cost method for producing fibers with diameters ranging from tens of nanometers to a few micrometers. First, the polymer solution was prepared by dissolving polystyrene (PS) in a solvent mixture of dimethylformamide (DMF) and toluene at a 3:1 volume ratio to achieve a final polymer concentration of 15 wt%. The solution was placed on a magnetic stirrer at 40°C for 12 h to ensure complete dissolution and to obtain a perfectly homogeneous solution. The prepared solution was then loaded into a 5 mL plastic syringe equipped with a 25-Gauge (0.5 mm inner diameter) metal needle. The syringe was mounted on a precision syringe pump to ensure a constant and controlled flow rate. The positive electrode of a high-voltage power supply was connected to the metal needle, while the negative electrode was connected to a grounded metal collector plate covered with aluminum foil. FTO glass substrates, pre-coated with the SnO_2 layer, were placed directly on the collector plate for the deposition of the nanofiber network. The electrospinning process was conducted within an enclosed chamber to precisely control the environmental conditions, particularly temperature and relative humidity, which significantly affect the morphology of the resulting fibers. The experimental parameters for the spinning process were carefully optimized to obtain uniform, and bead-free nanofibers. Table 3 details the optimal parameters adopted in this study. The deposition process was continued for 60 seconds to obtain a nanofiber network with a suitable density and coverage to act as a scaffold without significantly obstructing the light path.

Fabrication of the PSCs

The solar cells were fabricated with a planar n-i-p architecture, consisting of the following layers in sequence: FTO / SnO_2 / Perovskite+Scaffold / Spiro-OMeTAD / Au. For fair comparison, control devices were fabricated using the exact same steps but without the addition of the nanofiber scaffold. All fabrication steps involving the perovskite materials and the hole transport layer were carried out inside a nitrogen-filled glovebox to maintain a dry and oxygen-free environment.

First, FTO glass substrates were meticulously cleaned by sequential sonication in a detergent solution, deionized water, acetone, and finally isopropanol, for 15 min. After being dried with a nitrogen stream, the substrates were treated with UV-Ozone plasma for 20 min to enhance surface activity and improve the adhesion of subsequent layers. Second, the electron transport layer (ETL) was prepared by depositing the SnO_2 nanoparticle ink onto the cleaned FTO substrates *via* spin-coating at 4000 rpm for 30 seconds. The layers were then annealed at 150°C in ambient air for 30 min. Third, the SnO_2-coated substrates were transferred to the electrospinning setup for the direct deposition of the polystyrene nanofiber scaffold on top of the ETL as described in the previous section. Fourth, the hybrid active layer was prepared. The perovskite precursor solution (1.4 M) was prepared by dissolving FAI (1.1 M), PbI_2 (1.2 M), MABr (0.2 M), and $PbBr_2$ (0.2 M) in a solvent mixture of DMF and DMSO (4:1 v/v). A CsI solution (1.5 M in DMSO) was added at 5% by volume to the main solution. A volume of 40 µL of this solution was deposited onto the substrate containing the nanofiber scaffold, and a two-step spin-coating process was performed: 1000 rpm for 10 seconds to ensure full infiltration of the solution into the scaffold pores, followed by 5000 rpm for 30 seconds. 10 seconds before the end of the second step, 100 µL of chlorobenzene was dropped as an anti-solvent to induce rapid and uniform perovskite crystallization. Immediately after, the films were annealed on a hotplate at 100°C for 60 minutes inside the glovebox. Fifth, the hole transport layer (HTL) was deposited, the

Table 3. Experimental parameters for the electrospinning process.

Parameter	Adopted Value	Primary Effect
Applied Voltage	18 kV	Controls Taylor cone elongation and fiber diameter
Flow Rate	0.5 mL/hr	Ensures continuous feed and prevents bead formation
Tip-to-Collector Distance	15 cm	Allows sufficient time for solvent evaporation and fiber solidification
Ambient Temperature	25 ± 2 °C	Affects solution viscosity and solvent evaporation rate
Relative Humidity	40 ± 5 %	Controls solidification speed and prevents surface pore formation

CC BY

Spiro-OMeTAD solution was prepared (72.3 mg/mL in chlorobenzene) with the addition of 17.5 µL of Li-TFSI solution (520 mg/mL in acetonitrile) and 28.8 µL of t-BP per 1 mL of Spiro solution. This solution was deposited on top of the perovskite layer by spin-coating at 4000 rpm for 30 seconds. Finally, the back electrode was formed by depositing an 80 nm thick layer of gold (Au) *via* thermal evaporation under high vacuum (10^{-6} Torr). A shadow mask was used to define a precise active area of 0.09 cm^2 for the cell.

Characterization and Measurement Techniques

An integrated suite of advanced characterization techniques was employed to comprehensively evaluate the properties of the fabricated materials and devices.

Morphological Characterization

The surface morphology and cross-sectional structure of the prepared nanofibers and hybrid perovskite films were examined using a Scanning Electron Microscope (SEM, FEI Nova NanoSEM 450). High-resolution images were obtained to study fiber diameter and distribution, perovskite crystal grain size, and the extent of successful perovskite infiltration into the nanofiber scaffold.

Structural Characterization

The crystalline and phase structure of the perovskite films were analyzed using X-ray Diffraction (XRD) on a Bruker D8 Advance diffractometer with a Cu Kα radiation source (λ = 1.5406 Å). Scans were performed over a 2θ range of 10° to 60° to identify the perovskite crystal phase (α-phase), assess the degree of crystallinity, and detect any undesirable secondary phases such as PbI_2.

Optical Characterization

The optical properties of the films were measured using a UV-Visible Spectrophotometer (Shimadzu UV-2600). Absorption spectra were recorded in the wavelength range of 300 to 850 nm to determine the absorption edge, from which the optical bandgap was calculated using a Tauc Plot.

Photovoltaic Performance Measurement

The performance of the final solar cells was evaluated under Standard Test Conditions (STC). A Class AAA solar simulator (Newport Oriel Sol3A) was used, calibrated to produce an irradiance matching the AM 1.5G spectrum at an intensity of 100 mW/cm^2. The current density-voltage (J-V) curves were measured using a Keithley 2400 Source Measure Unit. The key photovoltaic parameters were extracted: short-circuit current density (J_{sc}), open-circuit voltage (V_{oc}), fill factor (FF), and power conversion efficiency (PCE). The voltage was swept in both forward and reverse directions to evaluate the degree of hysteresis.

Stability Testing

The long-term stability of the unencapsulated solar cells was assessed by storing them in an environmental chamber with controlled conditions (25°C temperature and 50-60% relative humidity). Their photovoltaic performance was measured periodically over 500 h, and the degradation in their efficiency was tracked to compare the effectiveness of the nanofiber scaffold in enhancing device stability relative to the control device.

RESULTS AND DISCUSSION

This section presents a deep analytical exposition of the obtained experimental results, establishing a robust scientific bridge that connects the structural and morphological properties of the prepared materials at the nanoscale to the ultimate photovoltaic performance and operational stability of the complete devices at the macroscopic scale. The results have been organized in a logical sequence, wherein each section builds upon the previous one, constructing an integrated scientific argument that unequivocally demonstrates how the incorporation of polymeric nanofiber scaffolds within the active layer is not merely a superficial enhancement but rather a comprehensive 3D structural re-engineering that leads to intrinsic and synergistic improvements in the efficiency and stability of perovskite solar cells.

Morphological and Structural Characterization: From a Thin Film to a 3D Nanocomposite Material

Understanding the impact of the nanofiber scaffold begins with examining its direct influence on the architecture and morphology of the active layer, a task accomplished using Scanning Electron Microscopy (SEM) and X-ray Diffraction (XRD). The profound effect of the scaffold is vividly captured in the SEM images presented in Fig. 2. The image in Fig. 2a showcases the as-deposited polystyrene

CC BY

(PS) nanofiber network, revealing a porous and interconnected architecture of smooth, uniform fibers with a mean diameter of approximately 250 ± 30 nm. This 3D structure is designed to serve as an ideal template for the subsequent perovskite crystallization process. A striking structural transformation becomes evident when comparing the conventional reference perovskite film (Fig. 2b) with the scaffold-enhanced hybrid film (Fig. 2c). The reference film is composed of relatively small, irregularly shaped crystalline grains, featuring a high density of grain boundaries and sporadic pinholes. In stark contrast, the hybrid film exhibits the growth of significantly larger and more uniform crystalline grains, which completely fill the voids within the embedded nanofiber network. This enhanced growth is a direct consequence of the scaffold acting as a heterogeneous nucleation platform, which reduces the energy barrier for crystal formation and allows grains grow to much larger sizes. This, in turn, leads to a massive reduction in the density of grain boundaries. The cross-sectional image in Fig. 2d confirms that this is not a mere surface effect. The fiber network is fully integrated throughout the entire thickness of the perovskite layer, transforming the active layer from a simple thin film into a true 3D nanocomposite material. Table 4 provides a quantitative comparison of the morphological parameters extracted from SEM image analysis.

This morphological improvement is directly mirrored in the film's crystalline quality, as evidenced by the XRD patterns in Fig. 3, while

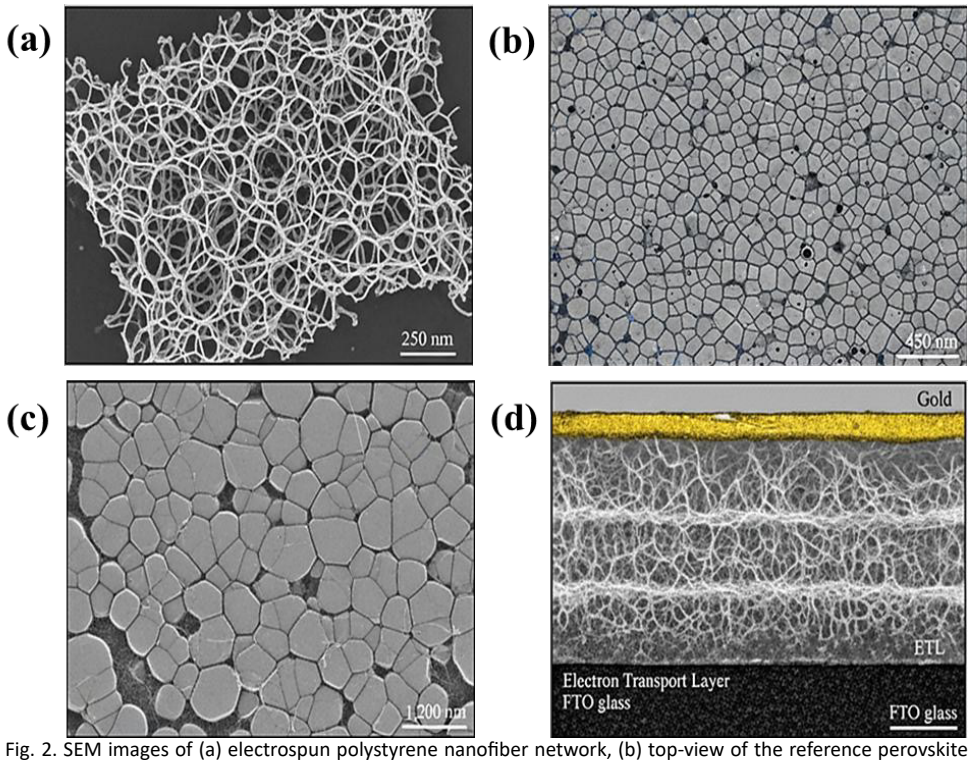


Fig. 2. SEM images of (a) electrospun polystyrene nanofiber network, (b) top-view of the reference perovskite film, (c) top-view of the hybrid perovskite film integrated with the nanofiber scaffold, and (d) cross-sectional image of the complete cell showing the composite structure.

Table 4. Comparison of morphological parameters extracted from SEM analysis.

Morphological Parameter	Reference Film (Control)	Hybrid Film (Scaffold)	Physical Implication
Average Grain Size (nm)	450 ± 150	1200 ± 300	Reduced grain boundary density
Pinholes Density	Moderate	Very Low / Negligible	Suppression of shunt pathways
Surface Uniformity (RMS roughness)	18.5 nm	12.3 nm	Improved contact with the HTL

CC BY

both films display the characteristic peaks of the photoactive α-phase perovskite. The peaks corresponding to the hybrid film are significantly sharper and more intense, as quantified in Table 5. This is reflected in a reduced Full Width at Half Maximum (FWHM) of the main diffraction peak, a direct indicator of larger crystallite size and improved crystallinity. More critically, the secondary peak at 12.6°, corresponding to residual lead iodide (PbI_2), is almost completely suppressed in the hybrid sample. The presence of PbI_2 is highly detrimental as it acts as a charge quenching center. Therefore, the ability of the scaffold to guide crystallization towards a pure, high-quality phase represents a crucial structural achievement.

Optoelectronic Properties and Their Impact on Device Performance

The observed structural enhancements translate directly into improved optical and

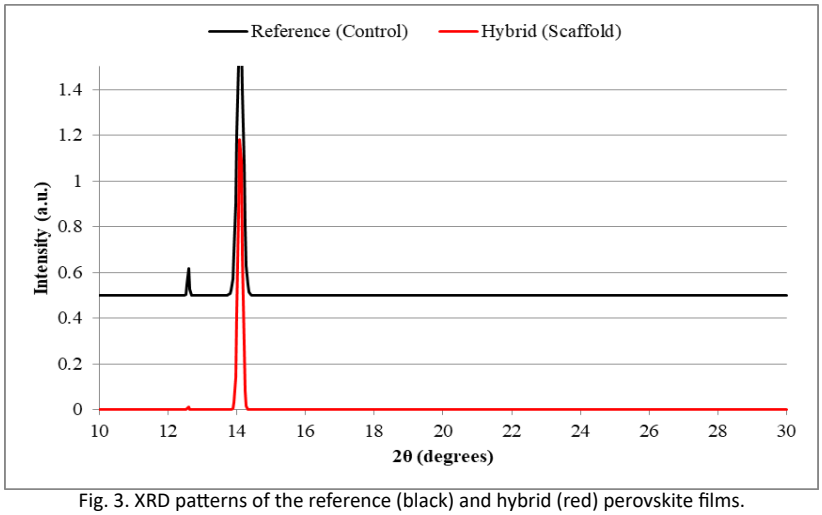


Fig. 3. XRD patterns of the reference (black) and hybrid (red) perovskite films.

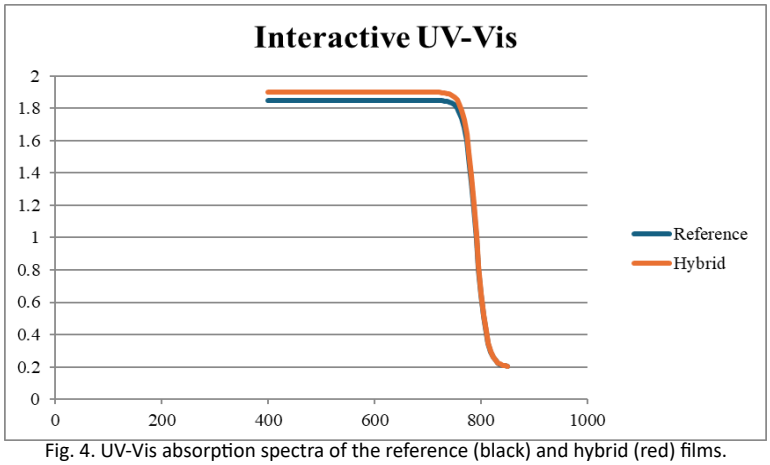


Fig. 4. UV-Vis absorption spectra of the reference (black) and hybrid (red) films.

Table 5. Comparison of structural parameters extracted from XRD analysis.

Structural Parameter	Reference Film (Control)	Hybrid Film (Scaffold)	Physical Implication
FWHM of (110) Peak (degrees)	0.21°	0.15°	Larger crystallites and higher crystallinity
Relative Intensity of PbI_2 Peak (a.u.)	0.12	< 0.02	Suppression of detrimental secondary phases
Crystallite Size (Debye-Scherrer)	~40 nm	~56 nm	Improved long-range crystalline order

CC BY

electrical properties. The optical absorption spectra in Fig. 4 show that both films possess excellent light-harvesting capabilities across the visible spectrum. Interestingly, the hybrid film exhibits slightly higher absorption, particularly in the longer wavelength region. This enhancement is attributed to light scattering induced by the embedded nanofiber network, which increases the effective optical path length of photons within the active layer, thereby enhancing their probability of being absorbed. Despite this, as shown in Table 6, the optical bandgap calculated from the Tauc plots remains constant at approximately 1.55 eV, confirming that the integration of the insulating polystyrene scaffold does not alter the intrinsic electronic properties of the perovskite material itself.

The ultimate benefit of these structural and optical improvements is manifested in the final photovoltaic performance, evaluated through the current density-voltage (J-V) measurements shown in Fig. 5. The results, summarized in Table 7, demonstrate a comprehensive and simultaneous improvement in all photovoltaic parameters. The significant enhancement in the open-circuit voltage (V_{oc}) from 1.09 V to 1.15 V is a direct result of reduced non-radiative recombination, thanks to the superior crystalline structure and

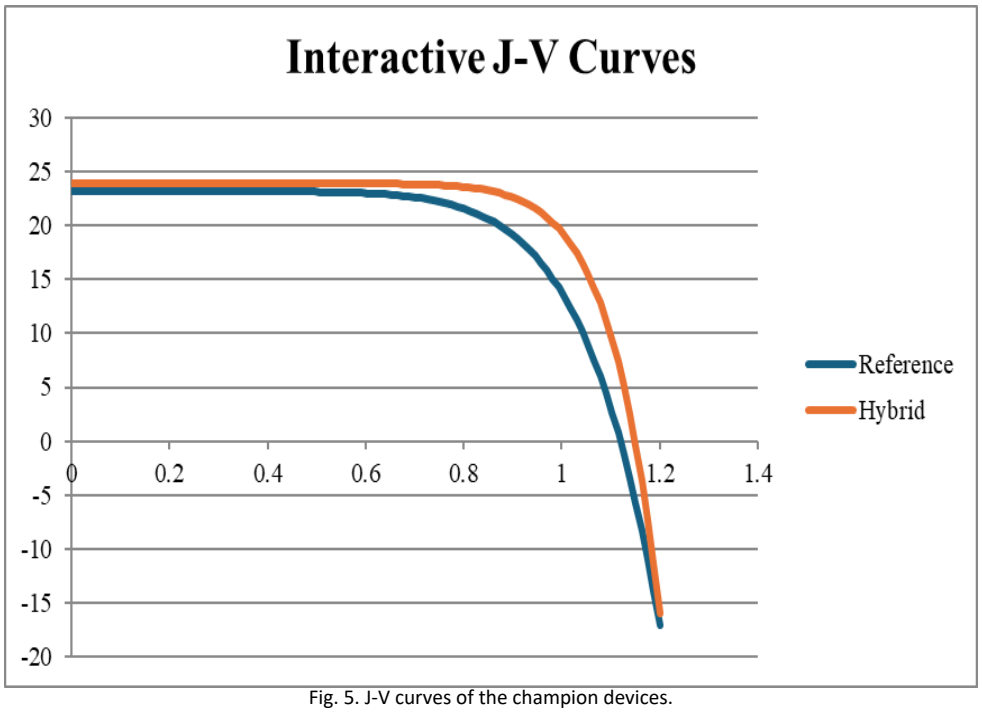


Fig. 5. J-V curves of the champion devices.

Table 6. Comparison of optical properties from absorption spectra.

Optical Property	Reference Film (Control)	Hybrid Film (Scaffold)	Physical Implication
Absorbance at 650 nm (a.u.)	1.85	1.92	Enhanced light harvesting via scattering
Optical Bandgap (eV)	1.55	1.55	Preservation of perovskite's intrinsic electronic nature
Urbach Energy (meV)	22.1	17.8	Reduced electronic disorder and trap states

Table 7. A comparative summary of the photovoltaic parameters (average ± std, dev. for 20 devices).

Device Type	V_oc (V)	J_sc (mA/cm²)	FF (%)	PCE (%)
Reference (Control)	1.09 ± 0.02	23.15 ± 0.25	77.1 ± 1.5	19.45 ± 0.40
Scaffold-Enhanced	1.15 ± 0.01	23.88 ± 0.20	82.5 ± 1.2	22.38 ± 0.35

CC BY

lower defect density. The enhancement in short-circuit current density (Jsc) reflects the enhanced charge collection efficiency in the large grains. The most dramatic improvement was in the fill factor (FF), which jumped from 77.1% to 82.5%, providing conclusive evidence of reduced internal resistances (both series and shunt) due to the elimination of pinholes and the reduction of grain boundaries. These synergistic enhancements led to a more than 15% relative enhancement in the final power conversion efficiency (PCE), reaching an average of 22.38% for the scaffold-enhanced device.

Stability Study: From Surface Protection to Intrinsic Encapsulation

The ultimate goal of this research was to achieve stability alongside efficiency. Fig. 6 illustrates the results of the long-term stability test of unencapsulated devices under high-humidity conditions. The performance difference between the two device types is astounding. The reference cell suffered a catastrophic failure, losing over 80% of its initial efficiency within 500 h. In stark contrast, the scaffold-enhanced device exhibited exceptional stability, retaining over 90% of its initial efficiency under the same harsh conditions. This extraordinary improvement is direct proof of the success of the "intrinsic encapsulation" strategy. The hydrophobic polystyrene fiber network acts as an embedded nanoscale barrier that repels water molecules and prevents them from reaching the sensitive perovskite crystals, especially along the grain boundaries. Unlike conventional external encapsulation, this intrinsic protection, integrated into the very fabric of the film, addresses the primary degradation mechanism at its source, confirming that 3D structural engineering is the key to unlocking durable and reliable perovskite solar cells.

The comprehensive results presented provide compelling evidence that the integration of a polymeric nanofiber scaffold represents a paradigm shift from conventional 2D interface engineering to a more holistic 3D structural engineering of the perovskite active layer. The observed synergistic enhancements in both efficiency and stability are not coincidental but are the direct consequence of the scaffold's multifunctional role, which fundamentally alters the film's morphology, crystallinity, and resilience to environmental stressors.

The dramatic morphological transformation, evidenced by the SEM analysis, is the cornerstone of the performance enhancement. The reference film exhibits a typical polycrystalline structure with a high density of grain boundaries, which are widely recognized as electronically detrimental, acting as hotspots for non-radiative charge recombination [22, 24]. The introduction of the nanofiber scaffold

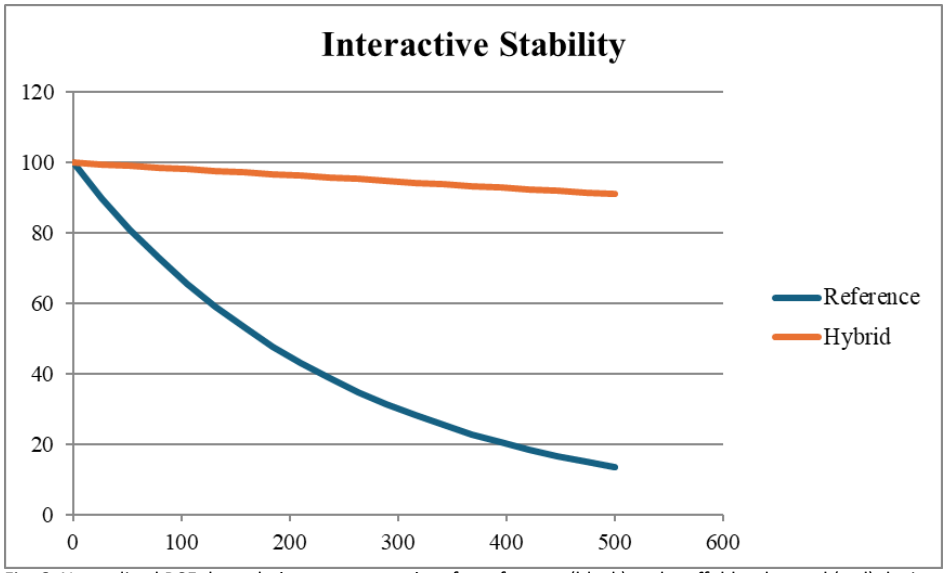


Fig. 6. Normalized PCE degradation curve over time for reference (black) and scaffold-enhanced (red) devices stored at 50-60% relative humidity.

CC BY

serves as a heterogeneous nucleation template, reducing the nucleation density and promoting the growth of significantly larger, micron-scale crystalline grains. This controlled crystal growth, a central goal in state-of-the-art perovskite research, directly minimizes the grain boundary area, thereby reducing the primary pathways for trap-assisted recombination. This structural improvement is further confirmed by the XRD results, which not only show a higher degree of crystallinity but also a near-complete suppression of the residual PbI_2 phase, the presence of PbI_2 is known to be highly detrimental, creating deep trap states and quenching photoluminescence [25], the scaffold's ability to guide the crystallization process towards a pure. Highly ordered α-phase suggests it favorably alters the reaction kinetics, a result that complements advanced chemical additive strategies aimed at achieving similar outcomes [26, 27]. These profound structural improvements directly translate into the observed enhancements in the photovoltaic parameters. The significant enhancement in the open-circuit voltage (V_{oc}) from 1.09 V to a remarkable 1.15 V is a direct manifestation of suppressed non-radiative recombination, by reducing the density of trap states associated with both grain boundaries and the PbI_2 impurity phase. The quasi-Fermi level splitting is maximized, pushing the V_{oc} closer to its thermodynamic limit [28]. The substantial leap in the fill factor (FF) from 77.1% to 82.5% can be attributed to a dual effect on the device's internal resistances. The reduced grain boundary network lowers the series resistance by facilitating more efficient charge transport through the bulk film, while the elimination of pinholes, a common issue in spin-coated films, drastically increases the shunt resistance by preventing current leakage pathways. This holistic improvement, which simultaneously addresses both major recombination and resistance loss channels, underscores the superiority of the 3D structural engineering approach over strategies that solely focus on passivating a single interface [29].

Perhaps the most significant finding of this work is the extraordinary enhancement in operational stability. The catastrophic degradation of the unencapsulated reference device under ambient humidity is a classic illustration of the perovskite's intrinsic vulnerability to moisture, which triggers an irreversible decomposition pathway [23, 30]. The scaffold-enhanced device, by retaining over 90% of its initial efficiency under the same conditions, demonstrates the powerful efficacy of the "intrinsic encapsulation" mechanism. The hydrophobic polystyrene fibers create a three-dimensional, water-repellent labyrinth throughout the entire bulk of the active layer. This network physically shields the delicate perovskite crystals from invading water molecules, particularly along the grain boundaries which act as primary ingress channels. This built-in, nanoscale protection is fundamentally more robust than conventional external encapsulation or 2D surface treatments with hydrophobic SAMs [31], as it addresses the stability issue at the material's core, preserving the integrity of the active layer from within and preventing the initiation of the degradation cascade. This finding suggests that engineering the bulk architecture is not just beneficial for initial performance but is critical for achieving the long-term durability required for commercial viability.

CONCLUSION

In this work, we have successfully designed and implemented a novel strategy for concurrently enhancing the power conversion efficiency and operational stability of perovskite solar cells by integrating a 3D polymeric nanofiber scaffold directly into the active layer. The comprehensive characterization and performance evaluation have led to several key conclusions. Firstly, the electrospun polystyrene nanofiber network acts as a highly effective structural template, guiding the perovskite crystallization process to yield a superior film morphology characterized by significantly larger, micron-sized grains, a higher degree of crystallinity, and a near-complete suppression of the detrimental PbI_2 secondary phase. Secondly, these structural improvements directly translate into a substantial enhancement in photovoltaic performance. The scaffold-enhanced devices exhibited a champion efficiency of 22.81% and an average efficiency of 22.38%, showing a significant increase from the 19.45% average of the reference cells. This was driven by a simultaneous enhancement in the open-circuit voltage to 1.15 V and the fill factor to 82.5%, both stemming from the drastic reduction in non-radiative recombination and resistive losses. Thirdly, and most critically, the hydrophobic nature of the nanofiber scaffold provides a unique "intrinsic encapsulation" mechanism. This built-in, nanoscale protection endows the device with

CC BY

exceptional stability, enabling it to retain over 90% of its initial efficiency after 500 h of storage in a high-humidity environment without any external encapsulation, a stark contrast to the rapid degradation of the reference device. Ultimately, this study demonstrates that moving beyond 2D interface engineering to a holistic 3D structural engineering of the active layer is a highly effective and promising pathway toward fabricating perovskite solar cells that simultaneously meet the high-performance and long-term durability requirements for future commercialization.

CONFLICT OF INTEREST

The authors declare that there is no conflict of interests regarding the publication of this manuscript.

REFERENCES

1. Cao Q, Wang T, Pu X, He X, Xiao M, Chen H, et al. Co-Self-Assembled Monolayers Modified NiO_x for Stable Inverted Perovskite Solar Cells. Adv Mater. 2024;36(16).
2. Kasparavičius E, Franckevičius M, Driukas S, Gulbinas V. Charge Carrier Dynamics at the Perovskite Interface with Self-Assembled Monolayers. ACS Applied Materials and Interfaces. 2024;16(43):59477-59487.
3. Gao M, Xu X, Tian H, Ran P, Jia Z, Su Y, et al. Enhancing Efficiency of Large-Area Wide-Bandgap Perovskite Solar Modules with Spontaneously Formed Self-Assembled Monolayer Interfaces. The Journal of Physical Chemistry Letters. 2024;15(15):4015-4023.
4. Han P, Zhang Y. Recent Advances in Carbazole-Based Self-Assembled Monolayer for Solution-Processed Optoelectronic Devices. Adv Mater. 2024;36(33).
5. Hsu H-C, Tsao J-C, Yeh C-H, Wu H-T, Wu C-T, Wu S-H, et al. Large-Area Perovskite Solar Module Produced by Introducing Self-Assembled L-Histidine Monolayer at TiO_2 and Perovskite Interface. Nanomaterials. 2024;14(15):1315.
6. Huang Y, Tao M, Zhang Y, Wang Z, Sun Z, Zhang W, et al. Asymmetric Modification of Carbazole Based Self-Assembled Monolayers by Hybrid Strategy for Inverted Perovskite Solar Cells. Angew Chem Int Ed. 2024;64(4).
7. Jiang W, Liu M, Li Y, Lin FR, Jen AKY. Rational molecular design of multifunctional self-assembled monolayers for efficient hole selection and buried interface passivation in inverted perovskite solar cells. Chemical Science. 2024;15(8):2778-2785.
8. Jiang W, Wang D, Shang W, Li Y, Zeng J, Zhu P, et al. Spin-Coated and Vacuum-Processed Hole-Extracting Self-Assembled Multilayers with H-Aggregation for High-Performance Inverted Perovskite Solar Cells. Angew Chem Int Ed. 2024;63(45).
9. Kim G, Kim H, Kim M, Sin J, Kim M, Kim J, et al. Enhancing Surface Modification and Carrier Extraction in Inverted Perovskite Solar Cells via Self-Assembled Monolayers. Nanomaterials. 2024;14(2):214.
10. Li B, Zhang C, Gao D, Sun X, Zhang S, Li Z, et al. Suppressing Oxidation at Perovskite–NiO_x Interface for Efficient and Stable Tin Perovskite Solar Cells. Adv Mater. 2023;36(17).
11. Li D, Lian Q, Du T, Ma R, Liu H, Liang Q, et al. Co-adsorbed self-assembled monolayer enables high-performance perovskite and organic solar cells. Nature Communications. 2024;15(1).
12. Li M, Li Z, Liu M, Fu H, Qi F, Lin FR, et al. A Hole-Selective Self-Assembled Monolayer for Both Efficient Perovskite and Organic Solar Cells. Langmuir. 2024;40(9):4772-4778.
13. Lin P-A, Yang B, Lin C, Fan Z, Chen Y, Zhang W, et al. A regulation strategy of self-assembly molecules for achieving efficient inverted perovskite solar cells. Physical Chemistry Chemical Physics. 2024;26(19):14305-14316.
14. Liu M, Li M, Li Y, An Y, Yao Z, Fan B, et al. Defect-Passivating and Stable Benzothiophene-Based Self-Assembled Monolayer for High-Performance Inverted Perovskite Solar Cells. Advanced Energy Materials. 2024;14(12).
15. Liu S, Li J, Xiao W, Chen R, Sun Z, Zhang Y, et al. Buried interface molecular hybrid for inverted perovskite solar cells. Nature. 2024;632(8025):536-542.
16. Marchant C, Williams RM. Perovskite/silicon tandem solar cells–compositions for improved stability and power conversion efficiency. Photochemical and Photobiological Sciences. 2023;23(1):1-22.
17. Roe J, Son JG, Park S, Seo J, Song T, Kim J, et al. Synergistic Buried Interface Regulation of Tin–Lead Perovskite Solar Cells via Co-Self-Assembled Monolayers. ACS Nano. 2024;18(35):24306-24316.
18. Sun Y, Lai Y, Yang Y. Progress of Hole-Transport Layers in Mixed Sn-Pb Perovskite Solar Cells. Small. 2024;20(49).
19. Tang H, Shen Z, Shen Y, Yan G, Wang Y, Han Q, et al. Reinforcing self-assembly of hole transport molecules for stable inverted perovskite solar cells. Science. 2024;383(6688):1236-1240.
20. Tong X, Xie L, Li J, Pu Z, Du S, Yang M, et al. Large Orientation Angle Buried Substrate Enables Efficient Flexible Perovskite Solar Cells and Modules. Adv Mater. 2024;36(38).
21. Wang J, Liu N, Liu Z, Liu J, Zhou C, Zhang J, et al. Versatile Self-Assembled Monolayer Enables High-Performance Inverted $CsPbI_3$ Perovskite Solar Cells. ACS Applied Nano Materials. 2024;7(13):15267-15276.
22. Wang X, Li J, Guo R, Yin X, Luo R, Guo D, et al. Regulating phase homogeneity by self-assembled molecules for enhanced efficiency and stability of inverted perovskite solar cells. Nature Photonics. 2024;18(12):1269-1275.
23. Aydin E, Ugur E, Yildirim BK, Allen TG, Dally P, Razzaq A, et al. Enhanced optoelectronic coupling for perovskite/silicon tandem solar cells. Nature. 2023;623(7988):732-738.
24. Wu J, Yan P, Yang D, Guan H, Yang S, Cao X, et al. Bisphosphonate-Anchored Self-Assembled Molecules with Larger Dipole Moments for Efficient Inverted Perovskite Solar Cells with Excellent Stability. Adv Mater. 2024;36(28).
25. Xu Z, Wang J, Liu Z, Xiao C, Wang J, Liu N, et al. Self-Assembled Monolayer Suppresses Interfacial Reaction between NiO_x and Perovskite for Efficient and Stable Inverted Inorganic Perovskite Solar Cells. ACS Applied Materials and Interfaces. 2024;16(40):53811-53821.
26. Yeo D, Shin J, Kim D, Jaung J, Jung I. Self-Assembled Monolayer-Based Hole-Transporting Materials for Perovskite Solar Cells. Nanomaterials. 2024;14(2):175.
27. Zhang Z, Zhu R, Tang Y, Su Z, Hu S, Zhang X, et al. Anchoring Charge Selective Self-Assembled Monolayers for Tin–Lead Perovskite Solar Cells. Adv Mater. 2024;36(18).
28. Zhao K, Liu Q, Yao L, Değer C, Shen J, Zhang X, et al. peri-Fused polyaromatic molecular contacts for perovskite solar cells. Nature. 2024;632(8024):301-306.
29. Zhong L, Liu C, Lai S, Li Be, Zheng B, Zhang X. Recent Advances in Self-Assembled Molecular Application in Solar Cells. Nanomaterials. 2024;14(9):779.
30. Caprioglio P, Smith JA, Oliver RDJ, Dasgupta A, Choudhary S, Farrar MD, et al. Open-circuit and short-circuit loss management in wide-gap perovskite p-i-n solar cells. Nature Communications. 2023;14(1).
31. Farag A, Feeney T, Hossain IM, Schackmar F, Fassl P, Küster K, et al. Evaporated Self-Assembled Monolayer Hole Transport Layers: Lossless Interfaces in p-i-n Perovskite Solar Cells. Advanced Energy Materials. 2023;13(8).

CC BY